International Journal of Heat and Mass Transfer 52 (2009) 1313–1325

Contents lists available at ScienceDirect

International Journal of Heat and Mass Transfer

journal homepage: www.elsevier.com/locate/ijhmt

Experimental investigation of forced and mixed convection heat transfer in a foam-filled horizontal rectangular channel

Irfan Kurtbas [a,*], Nevin Celik [b]

[a] University of Dumlupinar, Department of Mechanical Education, 43500 Kutahya, Turkey
[b] University of Firat, Department of Mechanical Engineering, 23279 Elazig, Turkey

ARTICLE INFO

Article history:
Received 23 May 2007
Received in revised form 25 February 2008
Available online 22 October 2008

Keywords:
Metal foams
Mixed convection
Porous media
Rectangular channel flow

ABSTRACT

An experimental study was performed to investigate the heat transfer characteristics of the mixed convection flow through a horizontal rectangular channel where open-cell metal foams of different pore densities (10, 20 and 30 PPI) were situated. A uniform heat flux was applied at all of the bounding walls of the channel. For each of three values of the uniform heat flux, temperatures were measured on the entire surfaces of the walls. Results for the average and local Nusselt numbers are presented as functions of the Reynolds and Richardson numbers. The Reynolds number based on the channel height of the rectangular channel was varied from 600 to 33000, while the Richardson number ranged from 0.02 to 103, extending over forced, mixed and natural convection. Second important parameter that influences the heat transfer is the aspect ratio of the foams. Three different aspect ratios (*AR*) as 0.25, 0.5 and 1 are tested. Based on the experimental data, new empirical correlations have been constructed to link the Nusselt number. The results of all cases were compared to that of the empty channel and the literature. We found that our results were in agreement with those that are mentioned in the literature.

1. Introduction

Porous media with high thermal conductivity have emerged as an effective method of heat transfer enhancement due to their large surface area to volume ratio and to intense mixing of the flow. Use of metal foams in heat transfer applications is novel. Consequently, numerous investigations have been carried out on this subject in the recent past. For instance, Leong and Jin [1] performed an experimental study focused on oscillating flow through a rectangular channel filled with open-cell metal foam. They used aluminum foams of 10, 20 and 40 PPI (pores per inch) as the porous media and presented data on pressure drops and velocities. Their results showed that the oscillating flow characteristics in an open-cell metal foam were governed by the kinetic Reynolds number $Re_{w(Dh)}$ based on a hydraulic diameter and the dimensionless flow displacement amplitude A_{Dh}. In a follow-on study [2], these authors used the same porous media to obtain the heat transfer performance of metal-foam heat sinks subjected to oscillating flows of various frequencies. The results for the length-averaged Nusselt number for both oscillating and steady flows indicated that higher heat transfer rates could be obtained in metal foams subjected to oscillating flow. Another application of metallic-foam porous media was investigated by Hetsroni et al. [3] in connection with a device for cooling transmission windows of an accelerator.

In other applications that appear in the literature, the metal foams were used in heat exchangers because of its high heat transfer capabilities. For example, Boomsma et al. [4] used open-cell metal foams as compact heat exchangers. It was shown that the open-cell metal foam heat exchangers gave rise to thermal resistances that are nearly one-third of the best available conventional heat exchanger. Zhao et al. [5,6] performed analytical studies of forced convection heat transfer characteristics of pipes filled with high-porosity, open-cell metal foam [5] and of foam-filled heat exchangers [6]. In the former study [5], it was shown that both the pore size and the porosity of metal foams played important roles in overall heat transfer performance. The latter study [6] showed that the thermal performance of a metal-foam heat exchanger could be superior to that of conventional finned-tube heat exchangers.

Tzeng et al. [7] investigated airflow passing through a rotating serpentine channel inside aluminum-foam material. The governing parameters were found to be the Prandtl, Reynolds, Grashof, and rotation numbers. Furthermore, they found that heat transfer between the fluid and solid phases was greater in the with-foam case than in the case without foam. For example, the Nusselt number increased by approximately 20% when foam was used.

Dukhan et al. [8] considered only one pore density, 10 PPI, in a one-dimensional numerical analysis of heat transfer in open-cell metal foams. The model combined conduction in the ligaments

* Corresponding author. Tel.: +90 274 5137917/125; fax: +90 274 5137917.
E-mail addresses: ikurtbas@gmail.com (I. Kurtbas), nevincelik23@gmail.com (N. Celik).

0017-9310/$ - see front matter © 2009 Published by Elsevier Ltd.
doi:10.1016/j.ijheatmasstransfer.2008.07.050

Nomenclature

D_h	channel hydraulic diameter, 2HW/(H+W),m
G	gravitational acceleration, m/s^2
Gr_{Dh}	Grashof number based on the channel hydraulic diameter
h	heat transfer coefficient, W/m^2 K
H	channel height, m
I	current, (amp)
k_{air}	thermal conductivity of air, W/m K
K	permeability, m^2
L_f	length of the aluminum foam, m
L	length of the channel, m
n	number of the temperature on the surface
Nu_{Hi}	local Nusselt number,
$\overline{Nu}_H$	average Nusselt number,
Pr	Prandtl number
Re_H	Reynolds number based on the channel height
Ri_{Dh}	Richardson number
T	temperature, °C
T_w	mean surface temperature, °C
V	mean air velocity m/s,
W	width of the aluminum foam, m

Greek symbols

β	thermal expansion coefficient, 1/K
ε	porosity
μ	dynamic viscosity, kg/m s
ν	kinematic viscosity, m^2/s
θ	dimensionless temperature
ρ	density, kg/m^3
Δx	spacing between thermocouples, m

Subscripts

B	bulk
I	surface column index (i = 1,2,. . .,6)
In	inlet

and convection to the coolant passing through the pores. The analysis showed that the temperature decayed exponentially along the foam in the flow direction. Recently Tzeng and Cheng [9] have investigated the convective heat transfer and pressure drop in porous channels in which the flow enters the channel through a 90-deg turn. Aluminum foams with a porosity of 0.93 were used in that study, and the size of the aluminum foams was fixed. Their results showed that the wall temperature was a maximum where the entering flow impinges on the duct wall. Ould-Amer et al. [10] presented some numerical results for laminar forced convection cooling of heat generating blocks mounted on a wall in a parallel plate channel. The effect of insertion of a porous matrix between the blocks on the heat transfer was taken into account. The results showed that the insertion of the porous medium may enhance the heat transfer rate on the vertical sides of the blocks.

Table 1 summarizes existing studies of forced convection air flow and heat transfer in porous media situated in rectangular ducts with uniform wall heat flux. The table indicates the porous material and its geometry. In the forth column of the table is a list of Nusselt number correlations. Since the geometrical and operating conditions of the cited experiments varied widely, an exact comparison among the respective Nusselt number results is nearly impossible. For example, the definitions of the characteristic dimension in the Nusselt number varied widely; for example, the hydraulic diameter, the channel height, the cell diameter, and others.

Present work includes the heat transfer analysis of the flow passing through a rectangular channel in which aluminum foam plate is located. The channel is heated by uniform heat flux on the top and bottom sides of the channel, varying 1879, 4378, and 9560 W/m^2. Varying Reynolds number from 6×10^2 to 3.3×10^4 means both laminar and turbulent flow are considered as flow regions. Richardson number is selected in the range of 0.02–103, which indicates the existence of the natural, mixed and forced convection heat transfers.

2. Experimental study

2.1. Setup and procedure

The setup includes the air facility, test section and instruments. Air from the quiescent laboratory room is driven into the operators

Table 1
Summary of experimental work for forced convection heat transfer in air passing through a porous medium situated in a rectangular duct with uniform wall heat flux

Investigators	Porous Material	PPI	Correlation (Nu)	Notations and definitions
Tzeng and Jeng [9]	Al foam	10-40	$Nu_H = 21.1Re_H^{0.457}$	
Leong and Jin [13]	Al foam	40	$Nu_H = 12.3A_o^{0.95}Re_H^{0.31}$ $0.51Re_{Dp}^{0.38} for 10PPI$	A_0 is dimensionless maximum flow displacement,
Hsieh et al [14]	Al foam	10-20-40	$Nu = 0.44Re_{Dp}^{0.44} for 20PPI$ $0.63Re_{Dp}^{0.46} for 40PPI$	D_P is equivalent spherical diameter of porousmedia,
Tzeng [11]	Al foam	10	$Nu_H = 4.835Re_H^{0.52}$	
Noh et al [15]	Al foam	10	$Nu = 23.1Re_{Dh}^{0.4}Pr^{-0.1}Da^{0.09}$	
Calmidi and mahajan [16]	Al foam	5-10-20-40	$Nu = 0.52(\frac{Re_H}{\varepsilon H})^{0.5}Pr^{0.37}$ $0.76Re_D^{0.4}Pr^{0.37} 1 \leqslant Re_d \leqslant 4$	e is porosity of the porous heat sink
Zukauskas [17,18]	Copper and Steel Alloy	10-20-30-60	$Nu = 0.52Re_D^{0.5}Pr^{0.37} 4 \leqslant Re_d \leqslant 10^3$ $0.26Re_p^{0.6}Pr^{0.37} 10^3 \leqslant Re_d \leqslant 2x10^5$	Re_d is the local Reynolds number.d is shape factor ($d = (1 - e^{((1-\varepsilon)/0.04)})d_f d_f$ is fibre diameter of metal foam
Ichimia [19]	Ceramic foam	20	$Nu = 2.43Re_{Dp}^{0.4} 65 \leqslant Re_{Dp} \leqslant 457$	
Hwang et al [20]	Al foam	10	$Nu = 0.32Re_{Dp}^{0.6} 1900 \leqslant Re_L \leqslant 7800$	
Hwang et al [21]	Sintered bronze beads	None	$Nu = 0.081(1-\varepsilon)\varepsilon^2 Re_d^{1.35}Pr^{0.33}(D_p/d)^{0.35} for Re_d \leqslant 75$ $Nu = 21.65(1-\varepsilon)\varepsilon^2 Re_d^{0.59}Pr^{0.33} for Re_d \leqslant 350$	d is diameter of fiber or sphere of the porous heat sink

by means of a downstream-positioned blower. The air enters a long hydrodynamic development length (L/Dh ~ 100) in order to establish a well-defined velocity profile at its downstream end. The downstream end of the development section is mated to the inlet of the test section. The test section proper is a rectangular duct filled with a metallic porous medium. To provide geometric flexibility, the test section was designed to allow for cross-sectional aspect ratios of 0.25, 0.5, and 1. The length of the test section in the flow direction was held fixed at 62 mm. The downstream end of the test section was, in turn, mated to an extension of the test section walls, but without the porous medium. At the far end of the downstream section, an isolation device was installed to decouple any possible blower-motor vibration.

Heating of test section was accomplished on all of its bounding surfaces by means of a very tightly wrapped silicon-rubber-sheathed heating element. The heating element was backed by a sheet of 2-mm-thick extruded polystyrene insulation. As a further defense against extraneous heat loss, the entire ductwork including the test section and the upstream and downstream sections were carefully wrapped with a 100-mm-thick batt of fiberglass insulation (k = 0.038 W/m K) having an aluminized outer surface.

Temperatures were measured by thermocouples deployed along the center span of the upper and lower walls of the test section and its upstream and downstream extensions. The thermocouples (Type T, 0.3-mm-diameter) had been specifically calibrated before their installation (0.05%). At all thermocouple locations, the thermocouple junctions were pressed tightly against the outer surface of the respective walls. Among the thermocouples, 6 were positioned in the test section proper. All told, 12 were affixed to the walls of the apparatus. In addition, two thermocouples were used to measure the fluid bulk temperature, respectively positioned upstream and downstream of the heated test section. The thermocouple voltages were collected by ALMEMO 5990-0 datalogger and transmitted directly to a personal computer.

For the measurement of the mass flow rate, a dedicated instrumented section, situated downstream of the extended test section, was used. The instrumented section had been previously calibrated against a rotameter.

The porous medium that filled the test section is aluminum foam of three different geometric specifications: 10, 20, and 30 PPI. The foams are shown by scaled photographs in Fig. 1, and also detailed thermophysical parameters and dimensions are and presented in Table 2.

The measurements were conducted for steady state conditions. The maximum wall temperatures were kept constant at approximately 76 °C for each data run. The Reynolds number Re_H based on the channel height H varied from 6×10^2 to 3.3×10^4. The Richardson number varied over the range from 0.02 to 103.

2.2. Data reduction

In present paper, the average and local Nusselt number were determined as functions of parametric values of the Reynolds and Richardson numbers (or the Grashof number). The Prandtl number of air is virtually constant over the temperature range of the experiments.

The local Nusselt number may be defined as:

$$Nu_{H,i} = \frac{qH}{(T_{w,i} - T_{in})k_{air}} \quad (1.a)$$

where q is local heat flux from the wall to the flowing fluid (assumed uniform on all surfaces which bound the porous medium) and k_{air} is thermal conductivity of the air. The temperature $T_{w,i}$ is defined as:

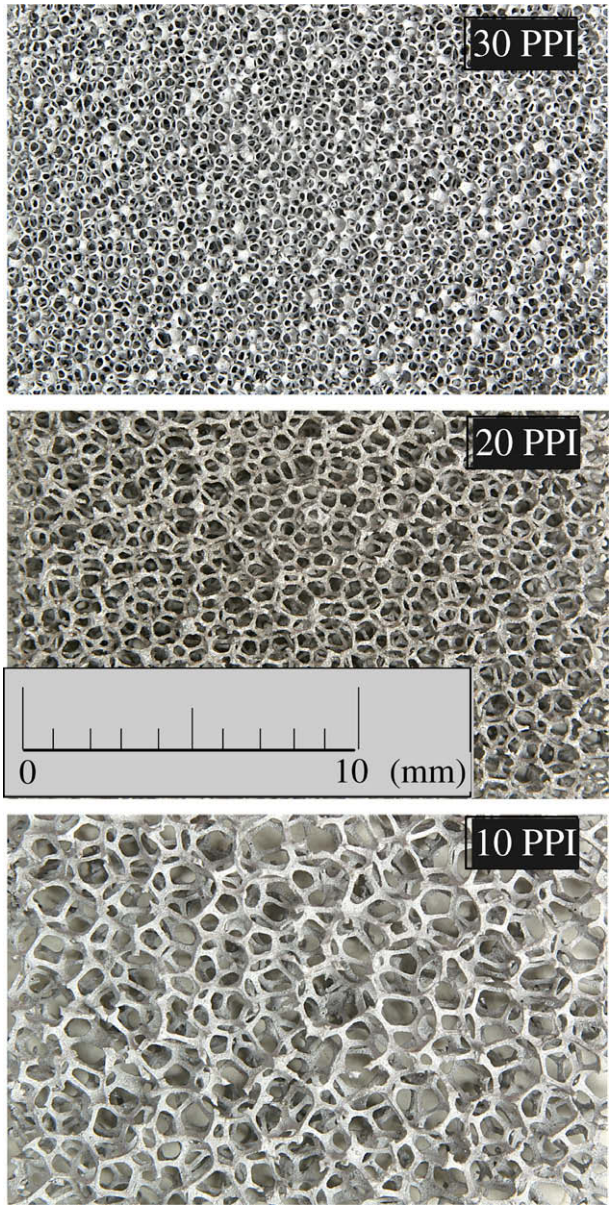

Fig. 1. Pictures of aluminum foam samples with various PPI values.

Table 2
Thermo-physical parameters and dimensions for aluminum foam

Pore density (PPI)	10	20	30
Materials	Al-6101	Al-6101	Al-6101
Porosity, ε	0.93	0.93	0.93
Permeability, K (m2)	1.04E-7	0.76E-7	0.63E-7
Legends, L_f (mm)	62	62	62
Width, W (mm)	52	52	52
Height, H (mm)	13	8	8

$$T_{w,i} = \frac{(T_{w,i})_{upper} + (T_{w,i})_{lower}}{2} \quad (1.b)$$

This definition takes cognizance of the fact that in a mixed convection flow, the temperatures at the upper and lower bounding surfaces may be different. The subscript i denotes the axial location at which the temperature is being measured.

The quantity T_{in} serves as a reference temperature to form the temperature difference in Eq. (1.a). It is the bulk temperature upstream of the inlet of the heated test section. The use of T_{in} as the reference temperature merits some discussion. The reason for choosing this reference temperature is to simplify, from the standpoint of a user, the application of the present results. In virtually all applications, the inlet bulk temperature is a known quantity. Therefore, it is convenient to use it in the evaluation of the present Nusselt number results to obtain the heat transfer coefficient. A second reason for using T_{in} as the reference temperature is that it provides continuity with results of previous investigations [7,9,11]. On the other hand, the use of the *local* bulk air temperature may present a problem in that it is not known *a priori* and, consequently, its use may complicate the evaluation of h.

The average Nusselt number was evaluated in accordance with the following definition:

$$\overline{Nu}_H = \frac{\int_0^L Nu_H dx}{\int_0^L dx} \cong \frac{\Delta x}{L}\sum_{i=1}^{n} Nu_H \tag{2}$$

where L is length of the test section; n is number of the temperature measurement points on the surface, Δx is the spacing between the two thermocouples.

Another quantity of practical utility is the temperatures on the bounding walls of the heated test section. A dimensionless temperature θ_w is defined as:

$$\theta_{w,i} = \frac{(T_{w,i} - T_{in})}{(qH)/k_{air}} \tag{3}$$

where T_w is defined in Eq. (1.b)

The total power dissipated by the silicone-rubber-encased heater may be represented by a heat flux q_{tot} by making use of the area of the heated surface. This heat flux may be subdivided into four components: (a) convective heat flux q to the flowing air, (b) radiative heat flux q_{rad} at the external surface of the insulation, and (c) natural convection $q_{natconv}$ at the external surface of the insulation. This energy balance is expressed by Eq. (5).

$$q = q_{tot} - q_{rad} - q_{natconv} \tag{4}$$

The sum of the last two terms of these equations is approximately 5%.

The Nusselt number results will be variously conveyed as functions of the Reynolds, Grashof and Richardson numbers, respectively defined as:

$$Re_H = \frac{\rho V H}{\mu} = \frac{\dot{m}}{\mu W} \tag{5}$$

$$Gr_{D_h} \equiv \frac{g\beta q \mathrm{Dh}^4}{k_{air}\nu^2} \tag{6}$$

$$Ri_{Dh} \equiv \frac{Gr_{D_h}}{Re_{Dh}^2} \tag{7}$$

where

$$Re_{Dh} = \left(\frac{D_h}{H}\right) Re_H \tag{8}$$

The fluid properties which appear in the foregoing equations were evaluated at the film temperature.

The uncertainty analysis, on the basis of 95% confidence level of errors, has been carried out using the method by Kline and McClintock [12]. The maximum uncertainties respectively associated with the Nusselt, Reynolds, and Grashof numbers are estimated to be 5.3, 3.2, and 5.8%.

3. Results and discussion

3.1. Average Nusselt number results

The variation of the average Nusselt number (Nu_H) versus the Reynolds number (Re_H) is depicted in Fig. 2 for 10, 20 and 30 PPI and AR = 1. As seen in the figure, the higher the pore density, the higher the average Nu. Another aspect demonstrated in Fig. 2 is

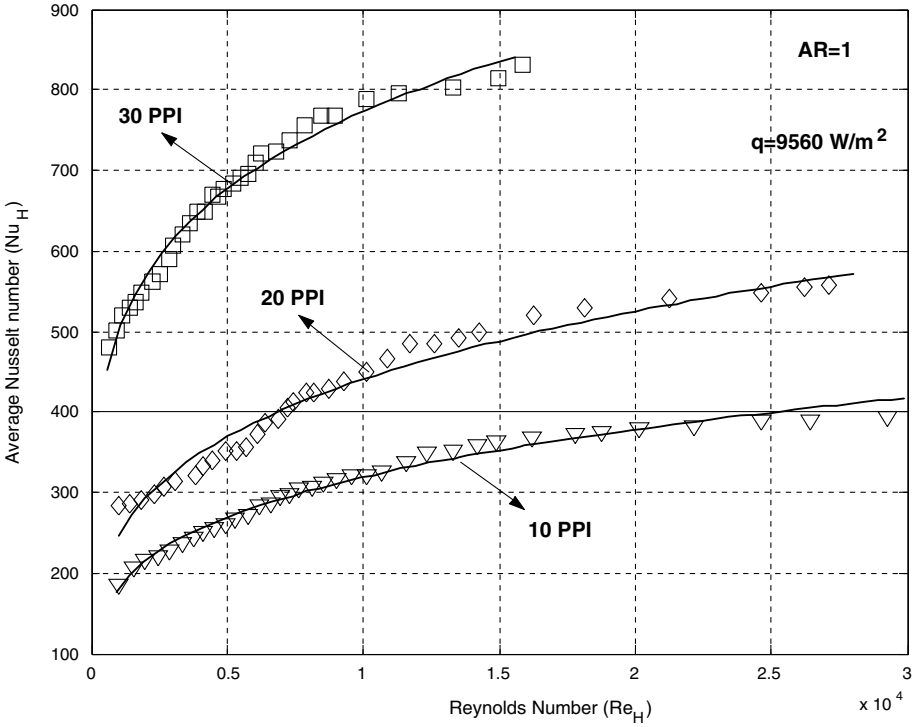

Fig. 2. Average Nusselt number (Nu_H) as a function of Reynolds number for AR = 1.

that: "the effect of Reynolds number on Nusselt number decreases, particularly at high Reynolds numbers ($Re_H > 10^4$)". It is observed that the effect of Reynolds number (Re_H) on average Nusselt number decreases for 10 PPI when Re reaches the value of 9×10^3, and a similar trend occurs for 20 and 30 PPI when Re reaches the value of 8×10^3. The average Nusselt number increases up to 74% when Reynolds number increases from 900 to 9×10^3. However, average Nusselt number increases approximately 21% when Reynolds number increases from 9×10^3 to 3.1×10^4. Although a similar trend is found for 20 and 30 PPI, this effect is shown at low Reynolds number (approximately 8×10^3). Likewise, the pore density has an important influence on the average Nusselt number. If the pore density increases from 10 PPI to 20 PPI, the average Nusselt number increases between 2% to 40% depending on Reynolds num-

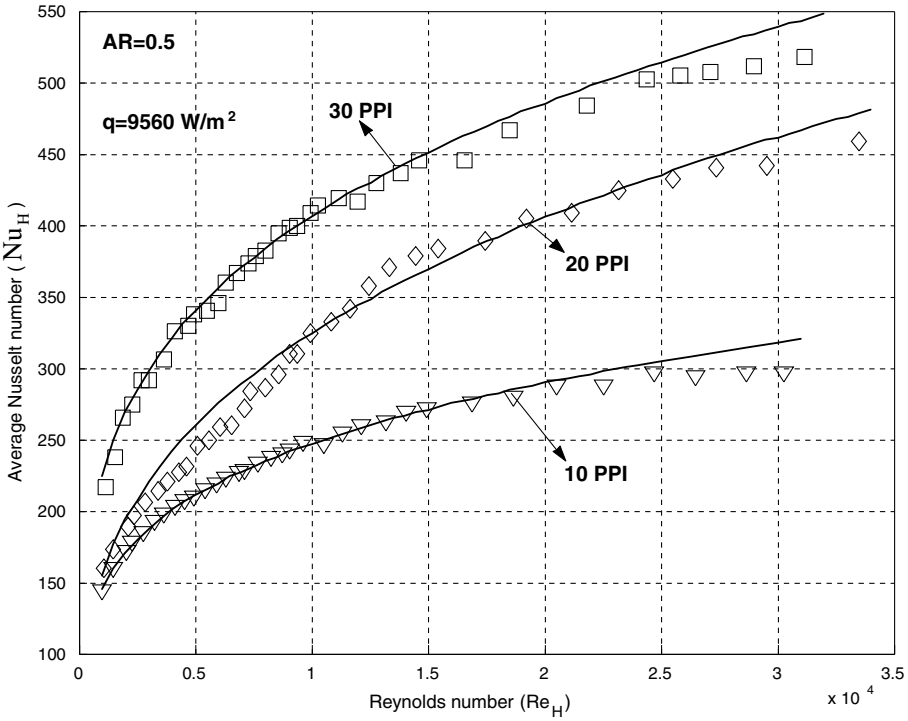

Fig. 3. Average Nusselt number (Nu_H) as a function of Reynolds number for $AR = 0.5$.

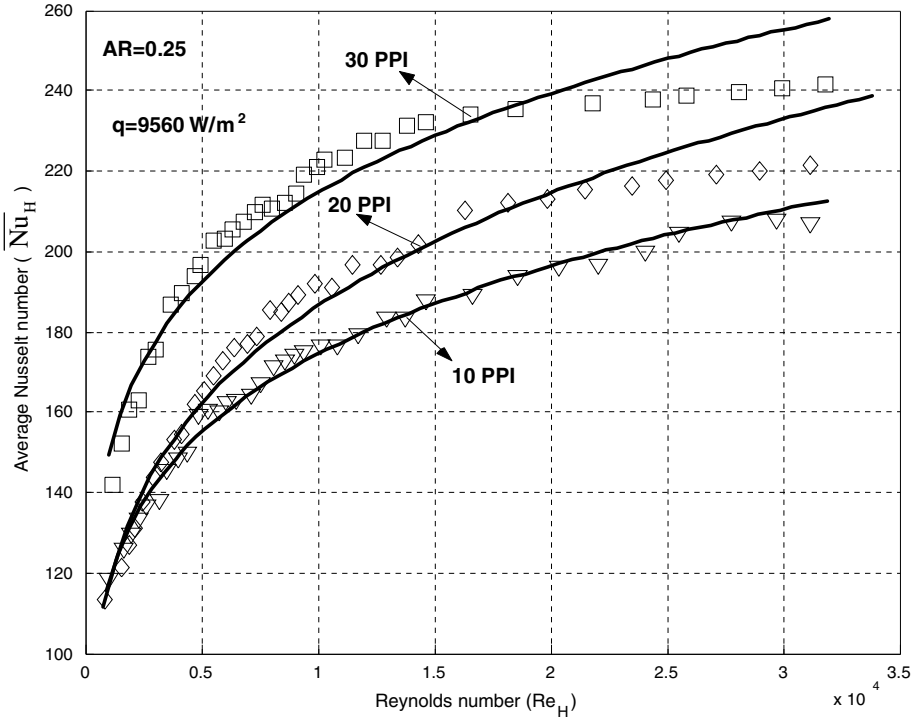

Fig. 4. Average Nusselt number (Nu_H) as a function of Reynolds number for $AR = 0.25$.

ber. However, average Nusselt number increases up to 145% when the pore density is increased from 10PPI to 30 PPI.

The aspect ratio also changes the effect of Reynolds number on the average Nusselt number (Figs. 3 and 4). For example, average Nu_H number has a sharp decrease at $Re_H = 1.7 \times 10^4$ for $AR = 0.5$, but when $AR = 0.25$ is considered, the decrement occurs at $Re_H = 2 \times 10^4$ (Fig. 3). In Fig. 3, the decline of Nu_H with respect to the decline of aspect ratio is plotted. When AR decreases from 1 to 0.5, the foam length causes a decrement in Nu number by 20% for 10 and 20 PPI, and for 30 PPI the decrement is about 45%. The decrease of the average Nusselt number is nearly 105% for the aspect ratio from 0.5 to 0.25 for 30 PPI, and all of these decreases follow a similar trend for all Reynolds numbers (Fig. 4).

Richardson number is the mixed convection parameter which shows the relative influence of natural convection compared to forced convection for a particular problem. Modified Grashof number (Gr_{Dh}) based on the hydraulic diameter and heat flux is used to obtain Ri number. As a consequence of the above mentioned experimental conditions, the Richardson number (Gr_{Dh}/Re_{Dh}^2) was obtained between 0.02 and 103. In this work, it is assumed that forced convection is dominant for $Ri \leqslant 0.1$ and natural convection is dominant for $Ri \geqslant 10$, because fully developed turbulent flows and laminar flow with low Grashof number have negligible buoyancy effects. The variation of the average Nusselt number versus Richardson number (Ri_{Dh}) is given in Fig. 4 for $AR = 1$.

If the definition mentioned above for the Nusselt number is considered, the average Nusselt number for forced convection must be the same even for different heat fluxes, because the term Nu is equal to the dimensionless temperature gradient at surface. From this point of view, the figure is an important criterion for validating the experimental procedure. As seen from Fig. 5, by decreasing the Richardson number, the effect of the buoyancy flow decreases for each pore density. For 10 PPI, the effect of Grashof number decreases by 2% at the value of $Ri_{Dh} = 0.2$. As can be observed from the above presentation, for $Ri_{Dh} \leqslant 0.2$, forced convection flow is dominant because $\overline{Nu}_H$ is nearly constant although the Richardson number changes. The region after value of $Ri_{Dh} = 0.2$ can be described as the mixed convection dominated region, even though $Ri_{Dh} > 10$. In other words, the natural convection is not completely dominant, even though $Ri_{Dh} > 10$. If the effect of Richardson number on Grashof number does not seem to change for different Grashof numbers, then natural convection is dominant in that region. However, the effect of Grashof number on $\overline{Nu}_H$ changes depending on the Richardson number for each pore density as seen from the figure. This circumstance indicates that forced convection affects $\overline{Nu}_H$ even though $Ri_{Dh} > 10$. Besides, increasing the pore density, buoyancy effect increases depending on the Richardson number. Nevertheless, after $Ri_{Dh} = 10$, the effect of the forced convection shows a decreasing trend.

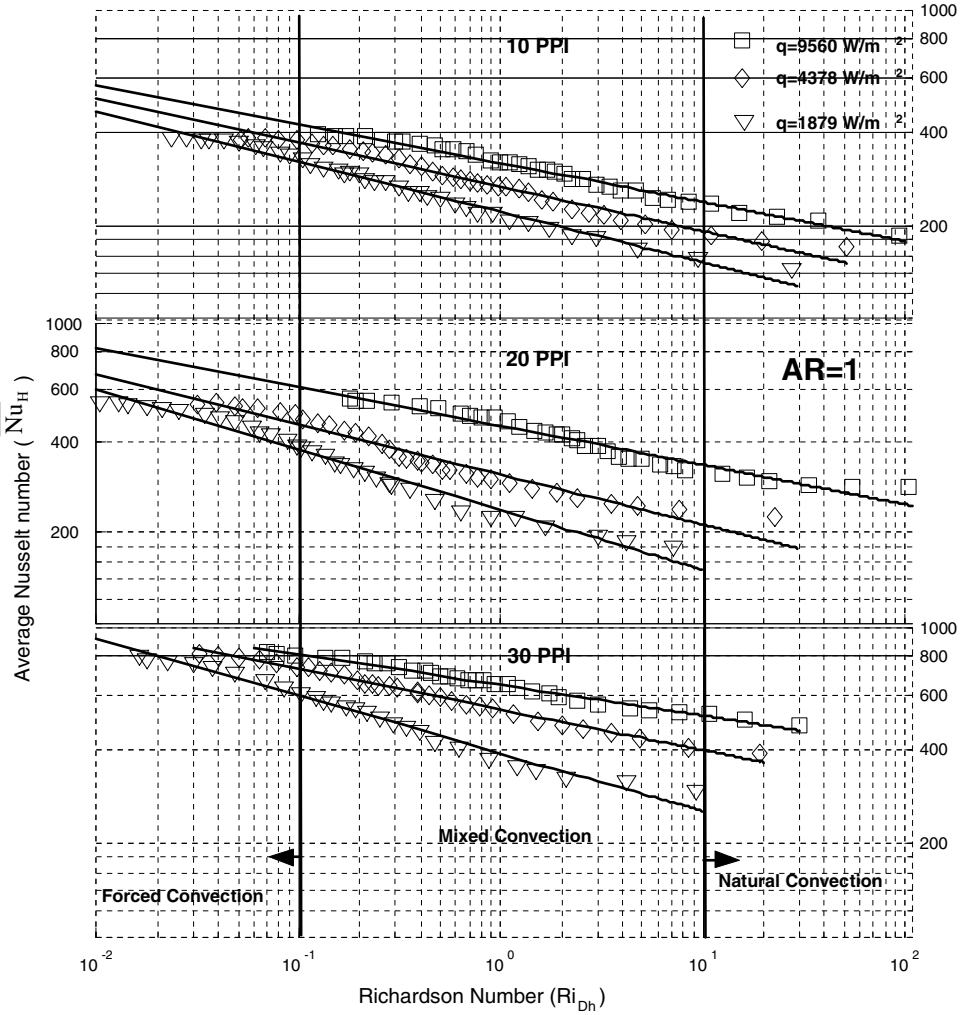

Fig. 5. Average Nusselt number (Nu_H) as a function of Richardson number for $AR = 1$.

3.2. Local Nusselt Number Results

Fig. 6 represents the local Nusselt number ($Nu_{H,i}$) for $AR = 1$ and each pore density (10, 20 and 30 PPI). Effects of changes in the Grashof number (Gr_{Dh}) on the local Nusselt number are also shown in Fig. 6. It can be seen that local Nusselt number increases with Grashof number and pore density. The figure reveals that the aluminum foams greatly improve heat transfer. Additionally, the pore density of the aluminum foam exhibits different thermal behaviors. As seen from the figure, the local Nusselt number has maxima at the channel inlet and slowly decreases through downstream. This behavior is exactly the same as that described in the prior research [11]. Besides, the local Nusselt number slowly decreases up to $x/L = 0.8$ for each pore density. After $x/L = 0.8$, it again slowly increases. This increase can be explained by considering the buoyancy-induced secondary flow and the effect of cell-velocity, which increases towards at the end of the foam. The local Nusselt number always increases with increasing Grashof number and the pore density due to the buoyancy effect. The Richardson number (Ri_{Dh}) is another important parameter which affects the heat transfer, and consequently, the buoyancy effect. As can be seen in Fig. 6, the local Nusselt number for $Ri_{Dh} \cong 0.1$ is always higher than that of $Ri_{Dh} \cong 1$ and $Ri_{Dh} \cong 10$. The buoyancy effects on the Nusselt number are more clearly shown in the figure. The buoyancy driven secondary flow has an important effect on the Nusselt number from the inlet to the middle of the channel for each pore density. The highest values of the Nusselt number are obtained for 30 PPI.

Fig. 7 plots the local Nusselt number for $AR = 0.5$. The figure shows clearly the effect of the aluminum foam on the heat transfer. It can be seen that the heat transfer decreases in the later part of the test section in which aluminum foam is absent (empty region). The Nusselt number is maximum at the channel inlet and slowly falls up to $x/L = 0.4$. After the distance $x/L = 0.4$, the Nusselt number decreases rapidly because of decreasing swirl intensity of the air, and the effect of increasing cell-velocity. After $x/L = 0.5$ where forced convection dominated flow occurs, the buoyancy-induced secondary flows decays, and no differences between distributions of the Nusselt number occur. For 10 PPI and $Ri_{Dh} \cong 0.1$, the Nusselt

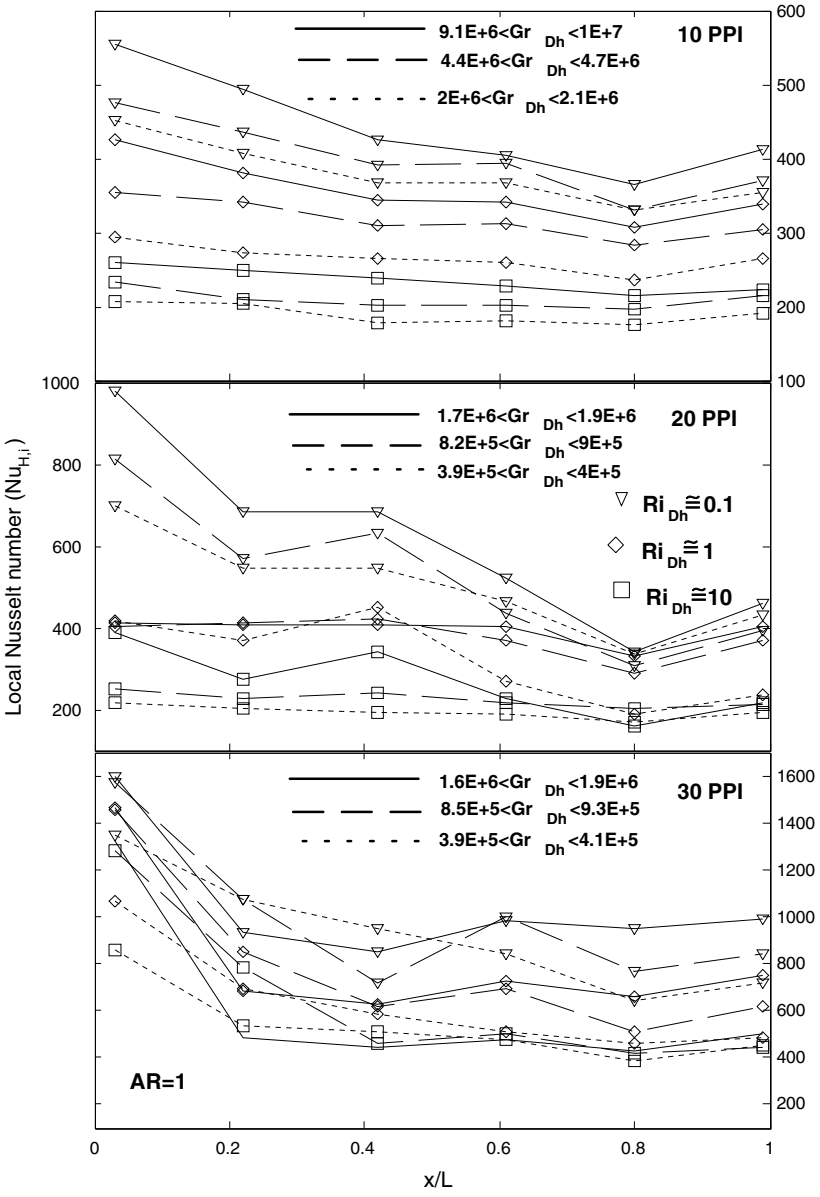

Fig. 6. Effect of Grashof number on local Nusselt number for $AR = 1$.

number at $x/L = 0.6$ is nearly 18% lower than that of at $x/L = 0.4$. The decrement percentages are 35% and 64% for 20 and 30 PPI, respectively. The results show that the Nusselt number obtained in the distance which is filled with aluminum foam is higher than that of the distance without foam. It can be concluded that at high Reynolds number and Grashof number, the effects of buoyancy-driven secondary flow on the Nusselt number increase. Also, the effect of the aluminum foam on the buoyancy-driven secondary flow becomes more important.

Fig. 8 presents the local Nusselt number distributions at various $\times$ values for $AR = 0.25$. Although a similar trend is shown in Fig. 7 and Fig. 8, the local Nusselt numbers obtained from $AR = 0.25$ are slightly different from the ones obtained at $AR = 0.5$. Nusselt number at $x/L = 0.25$, for 10, 20 and 30 PPI, are nearly 38%, 55% and 78% lower than that of at $x/L = 0.4$, respectively. It must be taken into consideration that at the end of the aluminum foam, the Nusselt number decreases more rapidly with increasing pore density. This circumstance is related to the effect of cell-velocity. The results indicate that the mean flow is forced to move at a relatively higher velocity at the end of the aluminum foam ($x/L = 0.25$). Nusselt number for 20 PPI, reduced from 484 to 226, under the conditions of $Gr_{Dh} \cong 1.6 \times 10^6$ and $Ri_{Dh} \cong 0.1$. For 30 PPI, under the conditions of $Gr_{Dh} \cong 1.8 \times 10^6$ and $Ri_{Dh} \cong 0.1$, Nusselt number seems to decrease from 662 to 218. This result is also based on cell-velocity, because the aluminum foam of 10 PPI allows continuing the buoyancy effect up to the end of test section. But, for 30 PPI, there is no substantial change in the Nusselt number after the distance $x/L = 0.4$. This can be attributed to the fact that the empty region is not affected much from the buoyancy-driven secondary flow, and is mainly affected by forced convection due to the mean flow velocity and cell-velocity.

Fig. 9 has been prepared similar to Figs. 6–8 in order to show more clearly the effects of the aspect ratio on the Nusselt number. The figure represents the Nusselt number for each aspect ratio and pore density at $Gr_{Dh} \cong 2 \times 10^6$ and $Ri_{Dh} \cong 0.1$. It is also clearly seen that local Nusselt number is individually different from each other

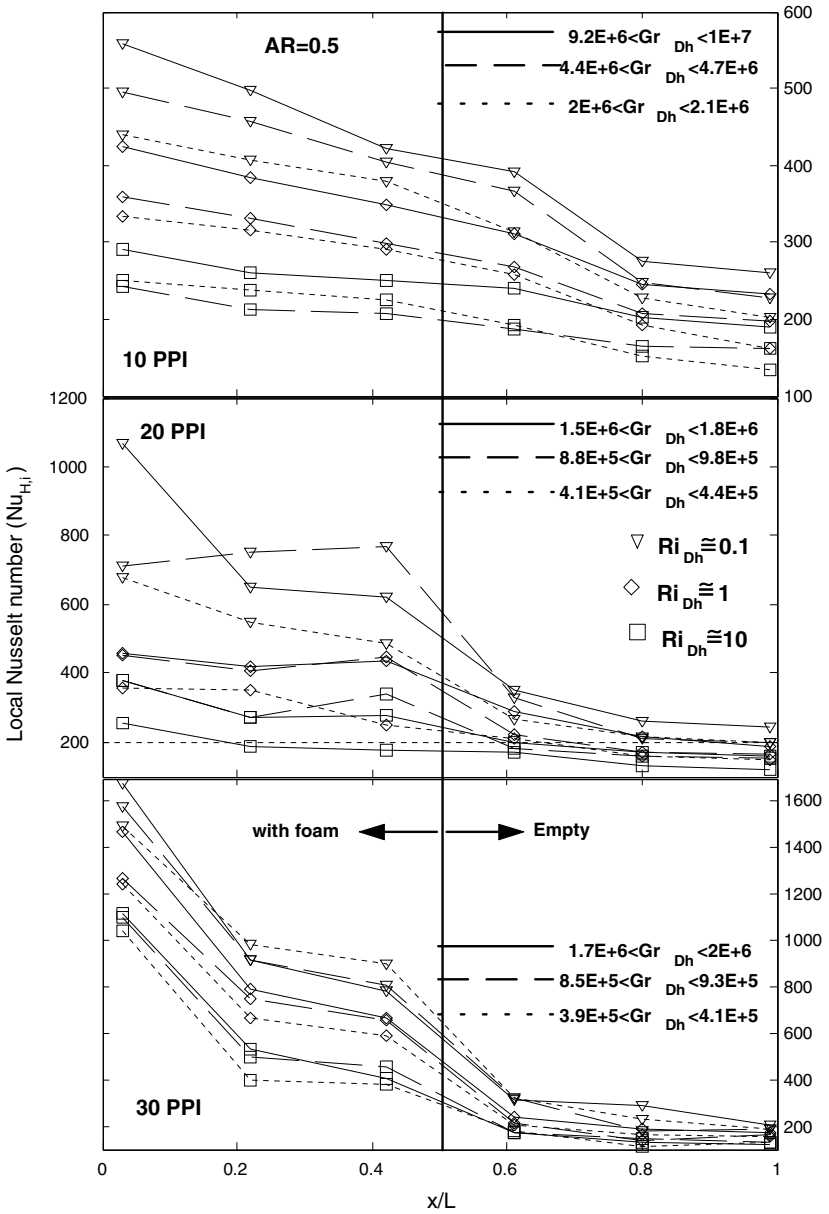

Fig. 7. Effect of Grashof number on local Nusselt number for $AR = 0.5$.

for even the same heat flux value as mentioned in Section 2.2. At the start of the tests, the authors suspected that the local Nusselt number in the region with aluminum foam might have the same value under the conditions of same heat flux and same Re number albeit without changing of aspect ratio. But, it is seen that the local value of the Nusselt number changes depending on the length of the aluminum foam at even the channel inlet. This case can be explained by two reasons: one is the fin effect of the aluminum foam; the other is due to the increase in the local velocity which changes depending on the aspect ratio of the aluminum foam in the channel.

3.3. Dimensionless temperature results

In Fig. 10, the ratio of heat transfer from top and bottom of the channel is shown. This ratio $((T_{w,i})_{upper}/(T_{w,i})_{lower})$ is a criterion for the buoyancy driven flow on both sides. In order to determine the heat transfer ratio, the local temperatures were measured on both top and bottom of the channel as mentioned in Section 2.1. This heat transfer ratio is given in terms of local surface temperature ratio in Fig. 10. If physical behavior of the natural convection is considered, the heat transferred by natural convection is from the bottom surface. It does not mean that the natural convection heat transfer completely occurs on the bottom surface. However, it is predicted that the forced convection heat transfer dominates on the top surface of the channel. As seen, in the entrance and exit region of the channel, the heat transfer variations show almost a forced convection balanced by buoyancy-driven secondary flow for 10 and 20 PPI and $AR = 1$. With increasing the pore density (30 PPI), the effect of the buoyancy driven flow slowly increases because the temperature differences increase with the increase in the pore density at $x/L = 0.03$ and 1. The trend is found to be similar in the variation of the ratio of surface temperature $((T_{w,i})_{upper}/(T_{w,i})_{lower})$ for each pore density. Fig. 10 reveals that the heat transferred from the bottom surface is more than that of the top surface. This is a result of the buoyancy forces, which is mainly accelerated

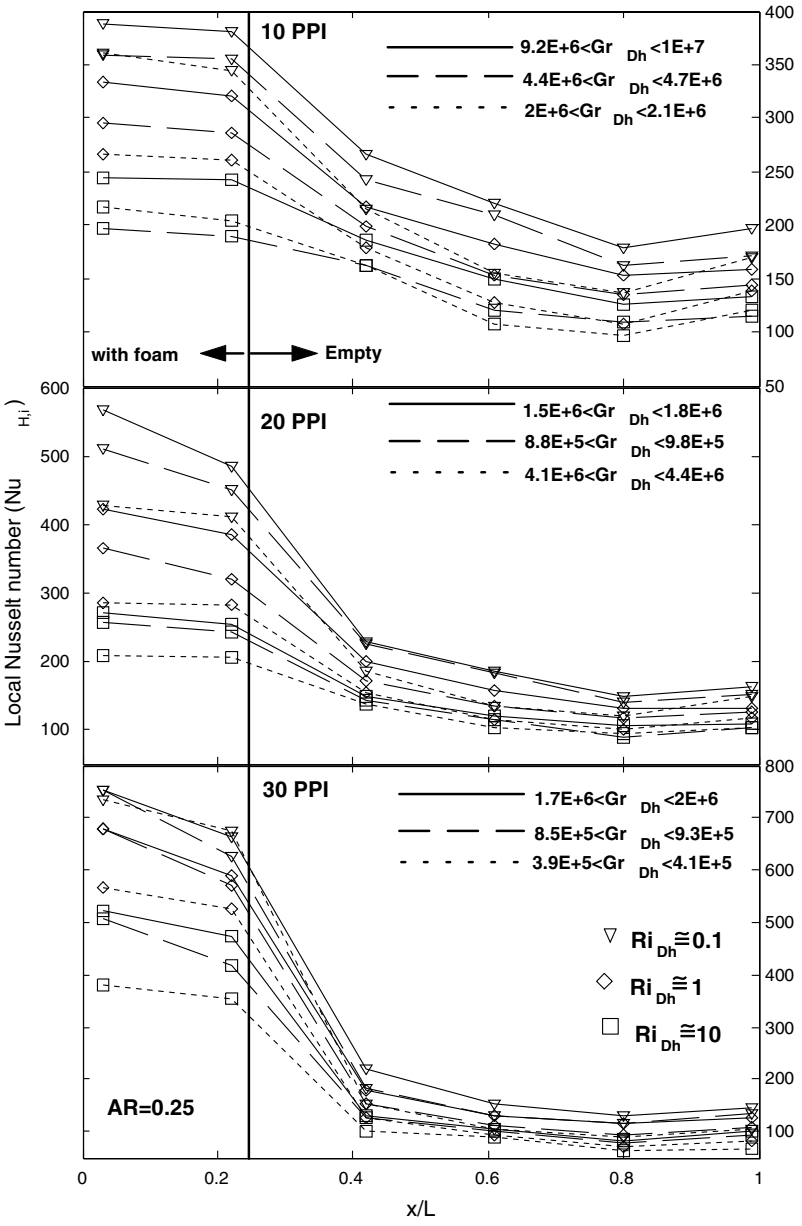

Fig. 8. Effect of Grashof number on local Nusselt number for $AR = 0.25$.

by the bottom surface. The most important parameters on the buoyancy driven flow are the pore density and Grashof number. The effect of the pore density on the ratio of the local temperatures $((T_{w,i})_{upper}/(T_{w,i})_{lower})$ is in the range of ca. 8–14%. The temperature differences indicate that the increase in the heat transfer from the bottom surface is around 14% higher than that of the top surface for 30 PPI with $Gr_{Dh} \cong 1.8 \times 10^6$ and $Ri_{Dh} \cong 0.1$.

Fig. 11 represents the local surface temperature ratio for three different aspect ratios (AR) and 30 PPI. As seen, the aspect ratio and the Grashof number have an important effect on the ratio of heat transfer between the top and bottom surfaces. The highest buoyancy driven flow is obtained for the highest aspect ratio ($AR = 1$) and Grashof number. The heat transferred from bottom surface is less than 5% than that of the top surface. However, even for $AR = 1$, the buoyancy driven flow on the bottom surface begins to lose its influence after the distance of $x/L = 0.3$. The most important parameter for buoyancy driven flow is the Grashof number in the region with and without the aluminum foam. In the region without aluminum foam, although buoyancy effect speedily falls between the distances of $x/L = 0.4$ and $x/L = 0.6$ for $AR = 0.5$, and between the distances of $x/L = 0.25$ and $x/L = 0.4$ for $AR = 0.25$, the buoyancy driven flow on the bottom surface is higher than that of the top surface, since; (i) the direction of the air changes locally due to untidy cell geometer of the aluminum foam, (ii) turbulent flows occur in the latter region of the aluminum foam although the cell-velocity relatively increases in the inlet and at the outlet of the aluminum foam. Hence, the heat transfer increases too. It can be clearly seen that at the distance $x/L = 0.7$, the ratios of top to bottom heat transfer obtained for $AR = 0.25$ are approximately equal to the values obtained for $AR = 0.5$. This circumstance is related to the relationship between the cell-velocity and mean air velocity; i.e. the influence of the cell-velocities decreases after the distance $x/L = 0.6$, and the mean air velocity dominates at that region for $AR = 0.25$. However, for $AR = 0.5$, cell-velocities dominate up to the end of the test section.

Fig. 12 shows the dimensionless temperature variation along the channel surface with porous medium. It is obvious that the temperature is its minimum level at the inlet and then it is rising along the channel length. Both the trend of the temperature distribution and values of the temperatures also have a good agreement with the Ref. [9].

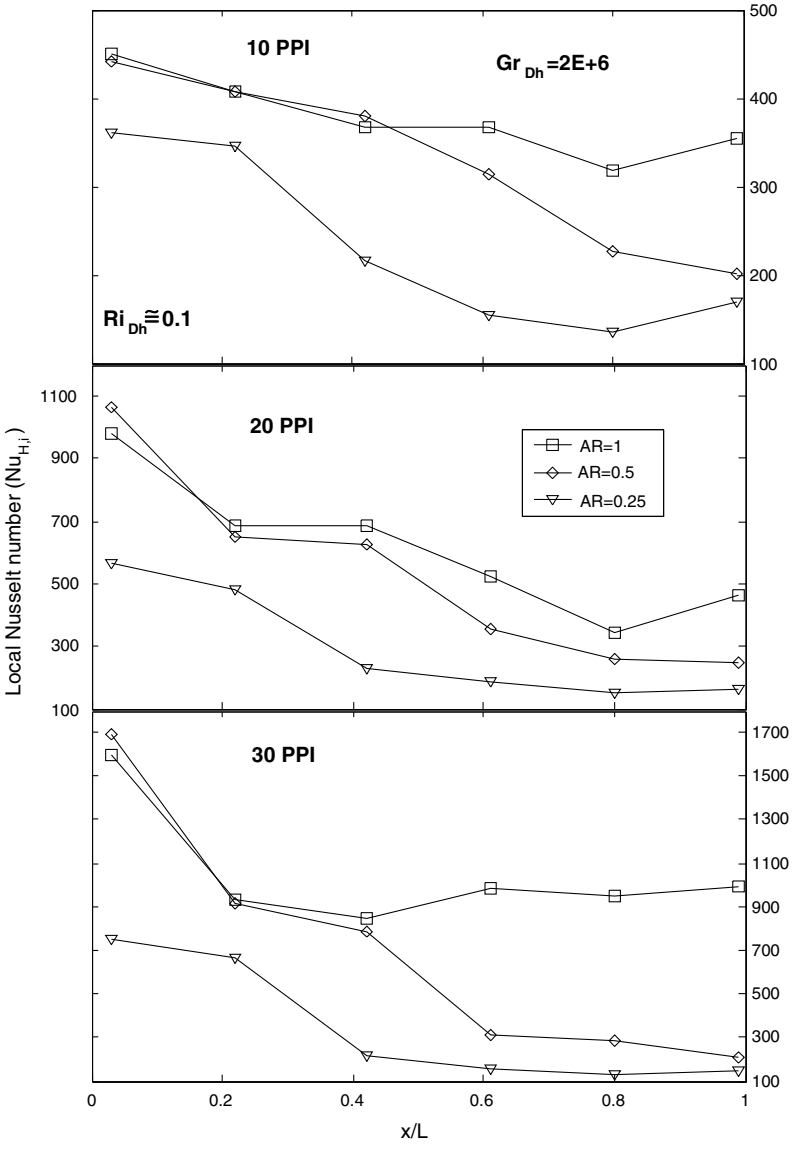

Fig. 9. Effect of aspect ratio on local Nusselt number for $Gr_{Dh} = 2 \times 10^6$ and $Ri_{Dh} = 0.1$.

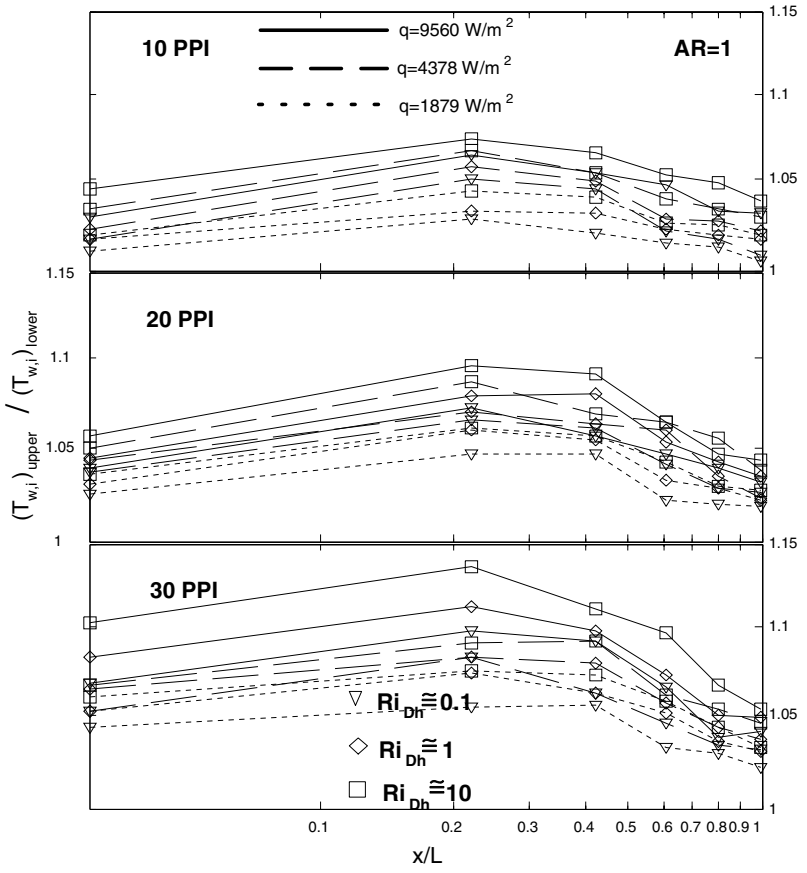

Fig. 10. Buoyancy-driven flow on the bottom surface of the channel for various *x* locations.

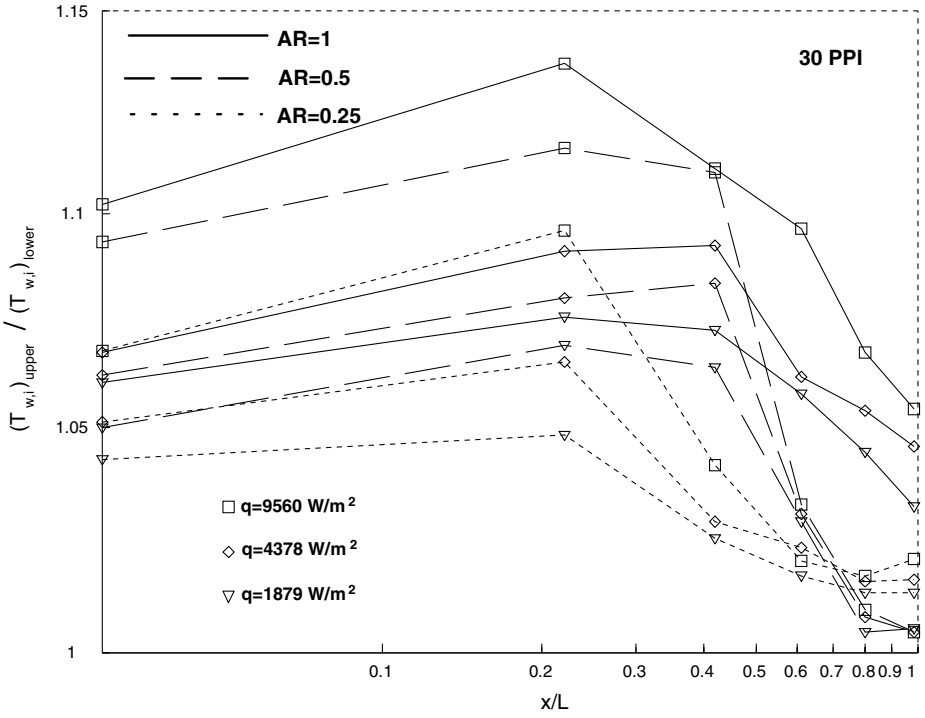

Fig. 11. Effect of aspect ratio on the buoyancy-driven flow from bottom surface for 30 PPI.

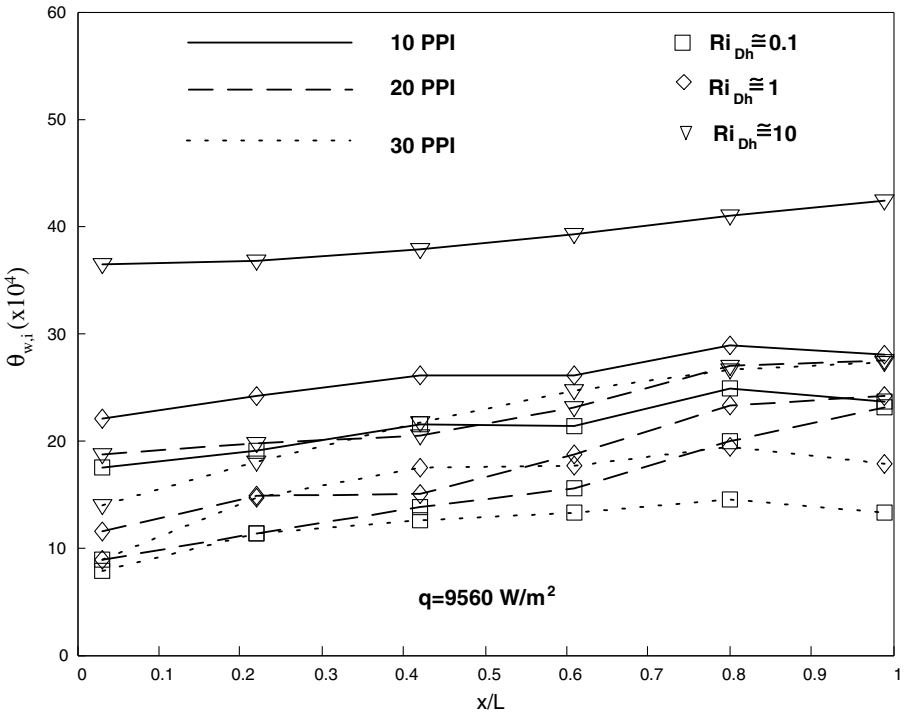

Fig. 12. Dimensionless wall temperatures for $q = 9560\ \mathrm{W/m^2}$ and $AR = 1$.

4. Conclusions

An experimental study was carried out for the case of assisting mixed convection in a rectangular horizontal channel heated top and bottom surface and filled with the aluminum foam. Enhancement of heat transfer from the aluminum foam under mixed convection conditions was investigated. The test fluid was air at room temperature. In this study, aspect ratio (AR) was varied from 0.25 to 1; pore densities (PPI) were 10, 20 and 30; Reynolds number (Re_H) varied from 6×10^2 to 3.3×10^4 and Grashof number (Gr_{Dh}) approximately varied from 10^5 to 10^7. We can extract concluding remarks from this study as follows:

- Average Nusselt number increases proportional to the pore density, in a horizontal rectangular channel which is filled with aluminum foam.
- Average Nusselt number increases very rapidly with respect to a critic value of Reynolds number. After this critic value, it slowly decreases. The critic value of Re_H can be changed according to pore density and aspect ratio of foam in channel; i.e., increasing aspect ratio can increase the critic Re number, on the other hand increasing pore density can decrease the critic value.
- Aspect ratio is proportional to Nusselt number.
- For high values of Gr_{Dh} and Re_H, local Nu_H numbers also increases to high levels.
- In present paper, Richardson number is in the range of 0.01–100. Almost for all pore densities, forced convection is dominant for $Ri_{Dh} < 0.1$. However, for $Ri_{Dh} > 10$, the effect of mixed convection still continues.
- For $AR < 1$, at the point where the metal foam ends, the local Nusselt number sharply decreases. This situation is explained by the cell velocity level. The larger the pore density is, the higher the cell velocity is.
- Increasing Gr_{Dh} number increases the buoyancy effects. The cell velocity is based on the pore density and the pore density itself has important effects on the buoyancy secondary flows.
- In the two cases of with foam and without foam, the buoyancy driven flows are effective on the bottom side of the channel.
- In the region with foam, due to two reasons, the heat transfer increases; (a) fin effect of foam and (b) the behavior of the foam as a turbulator. The pore density also contributes to this increment.

According to data obtained from this work, heat transfer increases especially for the foam of the highest pore density (30 PPI). For the aspect ratio $AR = 1$, and $Re_H < 8.10^3$, the use of foam has important advantages. In present study, the experiments are carried out for a limited range of Ri_{Dh} and Gr_{Dh}, due to the limited capacity of the fan and the AC power supply. The authors' opinion is that taking $Ri >> 1$ can be more useful in order to have more detailed data in the mixed convection region.

Acknowledgement

We would like to thank to Prof. E.M. Sparrow from University of Minnesota, for his scientific contributions and supervision.

References

[1] K.C. Leong, L.W. Jin, Characteristics of oscillating flow through a channel filled with open-cell metal foam, Int. J. Heat Fluid Flow 27 (2006) 144–153.
[2] K.C. Leong, L.W. Jin, Effect of oscillatory frequency on heat transfer in metal foam heat sinks of various pore densities, Int. J. Heat Mass Transfer 49 (2006) 671–681.
[3] G. Hetsroni, M. Gurevich, R. Rozenblit, Metal foam heat sink for transmission window, Int. J. Heat Mass Transfer 48 (2005) 3793–3803.
[4] K. Boomsma, D. Poulikakos, F. Zwick, Metal foams as compact high performance heat exchangers, Mech. Mater. 35 (2003) 1161–1176.
[5] W. Lu, C.Y. Zhao, S.A. Tassou, Thermal analysis on metal-foam filled heat exchangers. Part I: Metal-foam filled pipes, Int. J. Heat Mass Transfer 49 (2006) 2751–2761.
[6] C.Y. Zhao, W. Lu, S.A. Tassou, Thermal analysis on metal-foam filled heat exchangers. Part II: Tube heat exchangers, Int. J. Heat Mass Transfer 49 (2006) 2762–2770.
[7] S.C. Tzeng, C.Y. Soong, S.C. Wong, Heat transfer in rotating channel with open cell porous aluminum foam, Int. Commun. Heat Mass Transfer 31 (2) (2004) 261–272.

[8] N. Dukhan, P.D.Q. Ramos, E.C. Ruiz, M.V. Reyes, E.P. Scott, One-dimensional heat transfer analysis in open-cell 10-ppi metal foam, Int. J. Heat Mass Transfer 48 (2005) 112–5120.
[9] S.C. Tzeng, T.M. Jeng, Convective heat transfer in porous channels with 90-deg turned flow, Int. J. Heat Mass Transfer 49 (2006) 1452–1461.
[10] Y. Ould-Amer, S. Chikh, K. Bouhadef, G. Lauriat, Forced convection cooling enhancement by use of porous materials, Int. J. Heat Fluid Flow 19 (1998) 251–258.
[11] S.C. Tzeng, Spatial thermal regulation of aluminum foam heat sink using a sintered porous conductive pipe, Int. J. Heat Mass Transfer 50 (2007) 117–126.
[12] S.J. Kline, F.A. McClintock, Describing uncertainties in single-sample experiments, Mech. Eng. 75 (1953) 3–8.
[13] K.C. Leong, L.W. Jin, An experimental study of heat transfer in oscillating flow through a channel filled with an aluminum foam, Int. J. Heat Mass Transfer 48 (2005) 243–253.
[14] W.H. Hsieh, J.Y. Wu, W.H. Shih, W.C. Chiu, Experimental investigation of heat-transfer characteristics of aluminum-foam heat sinks, Int. J. Heat Mass Transfer 47 (2004) 5149–5157.
[15] J.S. Noh, K.B. Lee, C.G. Lee, Pressure loss and forced convective heat transfer in an annulus filled with aluminum foam, Int. Commun. Heat Mass Transfer 33 (2006) 434–444.
[16] V.V. Calmidi, R.L. Mahajan, Forced convection in high porosity metal foams, ASME J. Heat transfer 122 (2000) 557–565.
[17] A.A. Zukauskas, Convective heat transfer in cross-flow, in: S. Kakac, R.K. Shah, W. Aung (Eds.), Handbook of Single-Phase Convective Heat Transfer, Wiley, New York, 1987.
[18] W. Lu, C.Y. Zhao, S.A. Tassou, Thermal analysis on metal-foam filled heat exchangers. Part I: Metal-foam filled pipes, Int. J. Heat Mass Transfer 49 (15–16) (2006) 2762–2770.
[19] K. Ichimiya, A new method for evaluation of heat transfer between solid material and fluid in a porous medium, ASME J. Heat Transfer 121 (1999) 978–983.
[20] J.J. Hwang, G.J. Hwang, R.H. Yeh, C.H. Chao, Measurement of interstitial convection heat transfer and frictional drag for flow across metal foams, ASME J. Heat Transfer 124 (2002) 120–129.
[21] G.J. Hwang, C.C. Wu, C.H. Chao, Investigation of non-Darcian forced convection in an asymmetrically heated sintered porous channel, ASME J. Heat Transfer 117 (1995) 725–732.